Supplemental Information

Xiao Guo,[1,2,‡] Zhenrong Jia,[1,2,‡] Zijing Dong,[1,2,‡] Nikhil Kalasariya,[3] Jingcong Hu,[1,2] Zhuojie Shi,[1,2] Julian A. Steele,[4,5] Yi-Hsun Chen,[5] Gordon Ochsner,[6] Jinxi Chen,[1,2] Xiangkun Jia,[1,2] Yu-Duan Wang,[1,2] Ran Luo,[1,2] Ling Kai Lee,[2] Tao Wang,[1,2] Shunchang Liu,[1,2] Chao Luo,[1,2] Jia Li,[2] Martin Stolterfoht,[3] and Yi Hou[1,2,*]

[1]Department of Chemical and Biomolecular Engineering, National University of Singapore, Singapore, 117585, Singapore.

[2]Solar Energy Research Institute of Singapore (SERIS), National University of Singapore, Singapore, 117574, Singapore.

[3]Electronic Engineering Department, The Chinese University of Hong Kong, Sha Tin N.T., Hong Kong SAR, China.

[4]Australian Institute for Bioengineering and Nanotechnology, The University of Queensland, Brisbane, QLD, 4072, Australia.

[5]School of Mathematics and Physics, The University of Queensland, Brisbane, QLD, 4072, Australia.

[6]School of Chemical Engineering, The University of Queensland, Brisbane 4067 Queensland, Australia.

[‡]These authors contributed equally.

*Correspondence to: yi.hou@nus.edu.sg (Y.H.)

Materials

Lead chloride ($PbCl_2$, 99.999%), lead iodide (PbI_2, 99.99%), cesium bromide (CsBr, 99.999%), tetrakis-(dimethylamino) tin (IV) (TDMASn, 99.99%), 2-propanol (IPA, anhydrous), and dimethyl sulfoxide-d_6 (DMSO-d_6) were purchased from Sigma-Aldrich. Formamidinium iodide (FAI) was purchased from Greatcell Solar Materials. Silver pellets were purchased from Alfa Aesar. [4-(3,6-dimethyl-9H-carbazol-9-yl)butyl]phosphonic acid (Me-4PACz) were purchased from Tokyo Chemical Industry. C_{60} (99.9%) was purchased from Luminescence Technology. Lithium fluoride (LiF) was purchased from Kurt J. Lesker Company. PCE-10 and PDINN were purchased from 1-Material Inc.. P2EH-2V was synthesized following our previous work.**Error! Reference source not found.**

Wide-bandgap perovskite single-junction device fabrication

The patterned indium tin oxide (ITO) glass substrates were cleaned with a surfactant solution, then soaked in deionized water, acetone and IPA in the ultrasonic bath for 15 min each. After ultraviolet-ozone treatment for 15 min, the substrates were transferred to a N_2-filled glovebox and Me-4PACz (1 mg/ml in IPA) was spin-coated on the substrates at 4,000 r.p.m. for 30 s and heated at 100°C for 10 min. Then, the films were put into a perovskite evaporator in N_2-filled glovebox where PbI_2, CsBr, FAI (and $PbCl_2$ for Cl-doped condition) precursors are sublimed. The evaporation rates were monitored using quartz crystal microbalance sensors and kept constant by dynamically adjusting the source temperature throughout the deposition process. Specifically, the FAI rate is controlled at 1 Å/s, PbI_2 at 2 Å/s, and CsBr at 1.5 Å/s. For Cl-doped condition, $PbCl_2$ was sublimed as well and kept at 0.1 Å/s. The heating order of these materials follows $PbCl_2$, CsBr, PbI_2 and FAI, and the heating temperature of FAI is closely monitored to prevent a sudden increase of the rate, which is a sign for overheating and decomposition of the FAI material. Throughout deposition, the base pressure was constant at 1×10^{-5} mbar. The chamber and substrate temperatures were set to 20°C and rotation speed of substrate holder to 10 r.p.m.. The deposition is stopped when the thickness reached 320 nm. The total processing time for perovskite deposition is around 30 min. Without further post-treatments and annealing, the as-deposited perovskite thin-films were transferred to thermal evaporator where 20 nm of C_{60} was coated. Next, 10 nm of SnO_x is deposited in an atomic layer deposition (ALD) system with TDMASn and H_2O precursors. Finally, 100 nm Ag was thermally evaporated to complete the device fabrication.

Perovskite-OPV tandem device fabrication

After completing the deposition of SnO_x layer, the perovskite subcells were transferred to a sputter system, where ~5 nm ITO was sputtered as the charge recombination layer. After then, 30 nm MoO_x was thermally evaporated on top of ITO and the film was brought back to the N_2-filled glovebox where OPV precursor (D/A=1:1.5 (w/w), with a PCE-10 concentration of 7 mg/mL and 0.5% 1-Chloronaphthalene (v/v) as additive in chloroform) was spin-coated at 3,500 r.p.m. for 30 s and annealed at 100°C for 5

min. Next, PDINN was deposited by spin-coating its 1 mg/mL solution in methanol at 3,000 r.p.m. for 30 s. Finally, the film was transferred to thermal evaporator system to deposit 100 nm Ag as the top electrode to finish the tandem device fabrication process. Additionally, to reduce reflection loss of the incident light, a 90 nm LiF layer was evaporated on the glass side of the completed tandem device as an anti-reflection coating layer.

Device characterizations

Completed devices were masked with metal aperture masks (0.05 cm^2) for *J–V* measurements by a Keithley 2400 source meter under simulated 1-sun AM 1.5G illumination (100 mW cm^{-2}) with a Enli Technology solar simulator in a N_2-filled glovebox at 25°C. The solar simulator is calibrated by a built-in silicon reference cell integrated into the *J-V* testing setup from Enli Technology. The step size of *J-V* scans was set to be 20 mV with an integration time of 10 ms and a dwell time of 10 ms. Short-term MPP test was conducted on exactly the same setup and environment as the *J-V* measurement. Long-term MPP stability tests of the devices were conducted by an integrated 8-pixel MPP testing system (PURI Materials) under 100 mW cm^{-2} full spectrum (350-900 nm containing UV) white LED in a N_2-filled glovebox without (~45°C) or with active temperature controls (for 65°C MPP tests) with no encapsulation. Single-junction EQE measurements were conducted using a Bentham PVE300-IVT system. The intensity of the LED used was calibrated with built-in silicon and germanium diodes before measurements. For EQE tests of perovskite-OPV TSCs, we used a Quantum Efficiency Measurement System with voltage bias and multiple LED light bias from Enli Technology. The bias illumination was set at 850 nm and 450 nm for measuring perovskite subcell and OPV subcell of perovskite-OPV TSC, respectively. For the HREQE tests, the light was chopped at 137 Hz and coupled into a Bentham monochromator. The monochromatic light spot was focused onto the active area of the perovskite solar cell, and its current under short-circuit conditions was fed to a current preamplifier (Stanford SR 570) before it was analyzed with a lock-in amplifier (Stanford SR830 DSP). The time constant of the lock-in amplifier was chosen to be 1 s and the amplification of the preamplifier was increased to resolve low photocurrents. The EQE was determined by dividing the photocurrent of the cell by the flux of incoming photons, which was measured using a calibrated Si photodiode. All EQE measurements were conducted in an ambient atmosphere with a temperature of 25°C and ~60% relative humidity with encapsulation. Cross-sectional SEM images of devices were taken with Regulus SU8200 system (Hitachi) at 5 kV accelerating voltage under SE mode. Fast hysteresis *J-V* curves were obtained by pre-biasing the cells at a voltage just above the V_{OC} followed by a triangular voltage pulse from V_{OC} to -0.1 V to V_{OC} at variable frequencies or scan speeds. The duration of the hold voltage at V_{OC} was 5 times longer than the total scan time of the voltage sweep. The scan speed time of the voltage was thereby varied with a function generator, and the voltage response of the cell was measured with an oscilloscope using a system developed by FastChar UG. For the BACE measurements, the device is initially held at a voltage close to V_{OC}, where the injected charge equals to the J_{SC}. After the pre-bias, a bias of 0 V was applied to

extract the injected, ionic, and capacitive charge in the device. Finally, the extracted charge, which is not necessarily the same as the internal charge, was obtained by integrating the current transient and the charge carrier density by dividing the total charge by the elementary charge and the cell volume, which assumes a homogenous internal distribution.[S1] We note that if the distribution under the prebias is not uniform, but tilted, it will lead to deviations from the true ion density by the factor of d_{drift}/d, where d_{drift} is the average drift distance through the active layer (sum of electrons and holes), and d is the film thickness. The delay times for the fresh devices were chosen to be typically 4 times longer than the extraction time of charges observed under the collection bias (typically about 5 to 10 s) to allow ionic charges to distribute throughout the active layer during the prebias. The measurements were performed using the FastChar setup from SolarSense Technologies Ltd., which is based on an oscilloscope, as well as a Keithley 2400 source meter.

Material characterizations

UV-vis absorbance spectra were recorded with Agilent Cary 7000 spectrophotometer. The lamp was pre-heated for 30 min before conducting measurements. Steady-state PL and PL evolution measurements were done by LP20-32 radiative efficiency meter (Quantum Yield Berlin). The built-in 532 nm laser was switched on 15 min in advance to allow warmup and stabilization. All of PL spectra were recorded under 100 mW cm^{-2} 532 nm laser illumination. The confocal PL imaging was performed on a Nikon A1 confocal microscope using a 633 nm laser to excite wide-bandgap perovskite. The configuration of perovskite thin-films used for all PL-related measurements is ITO/perovskite. XRD patterns were recorded on a Bruker D8 Advance X-ray diffractometer with Cu Kα radiation (λ=0.1542 nm). XPS measurements were performed with the Kratos Axis Ultra XPS system. NMR was conducted on a Bruker Ascend 400 MHz spectrometer. FTIR was acquired on Thermo Scientific Nicolet iS50 spectrometer. For HAADF and STEM-EDX characterizations, cross-sectional sample of Cl-doped single-junction wide-bandgap perovskite solar cell was meticulously prepared using a dual-beam focused ion beam scanning electron microscopy (FIB-SEM) system (FEI Helios NanoLab 600). This system integrates both an electron beam gun and a gallium ion beam gun, with the latter operating within a voltage range of 1-30 kV to precisely section the samples. Meanwhile, the electron beam was maintained at 2 kV with a beam current of 0.86 pA to minimize potential damage. To further safeguard the perovskite structure, a protective multilayer coating was applied, consisting of an evaporated amorphous carbon (C) layer, a sprayed gold (Au) layer, and a deposited platinum (Pt) layer. HAADF-STEM imaging was performed using Spectra-300 spherical aberration-corrected TEMs, operated at 200 and 300 kV. The elemental distributions of the samples were characterized using a Super-EDX accessory on Spectra-300 microscope. The X-ray EDX was equipped with dual silicon drift windowless detectors, enabling high-sensitivity elemental mapping. For EXAFS measurements, Pb L_3-edge X-ray absorption spectra (XAS) were captured at the Australian Synchrotron (ANSTO in Clayton, Victoria) XAS beamline 12-ID. A double-crystal Si (111) monochromator equipped with focusing optics was used to reduce

harmonic content while producing excitation energy. The inline Pb metal foil was used to calibrate the monochromator at Pb-L_3 absorption edge with E0 set to its reported value of 13035.07 eV.[S2] All acquisitions were performed on powdered materials in a transmission mode. Perovskites powders were mixed with cellulose and pelletized as 7 mm diameter disks to mitigate absorption effects. Brief XAS scans of specific samples were conducted to verify the stability of the materials under at least several minutes of X-ray exposure before the full acquisitions. Samples were measured in a slew-scanning move with varying energy intervals over the pre-edge (5 eV) and the XANES region (0.25), with 0.035 intervals in k-space over the EXAFS. At low-k an integration time of 450 ms was employed per interval, with longer integration times weighted toward high-k portions of the spectrum, up to a maximum value of 16 in k-space (max of 1000 ms). For EXAFS data analysis, multiple scans were collected at different positions of the sample. Data processing including background subtraction, scan averaging, edge-height normalization, and rebinning was performed based on the Athena program.[S3] For normalization of energy spectra and removal of background, the pre-edge range was set between -170 eV and -50 eV, while the normalization range spanned from 150 to 1050 eV post-edge. The order of normalization was designated as 3. For the presented EXAFS data, the k-weight was configured as 2 or 3, and the k-range for the forward Fourier transform was defined from 1.5 to 10.

EXAFS fitting was conducted in the ARTEMIS, part of the IFEFFIT software package.[S3] The scattering paths used to evaluate and model the data were derived from the optimized crystal structures of $FAPbI_3$ and $FAPbBr_3$ perovskite considering the different nearest neighbor Pb-X paths. Using these input structures to derive the scattering paths, an agreeable fine structure accounting the for dominant EXAFS signal arising from an R fitting window of 1.5 to 3.5 Å emerged. The data were ultimately fit using 16 variables and 22 independent points, resulting a reasonable R-factor of 0.011. The fitting was conducted in R-space using multiple k-weightings, with k = 1, 2 and 3. Errors of individual fit parameters were determined using ARTEMIS to take into account the correlations between parameters and known parameters without error estimates were fixed during the fit.

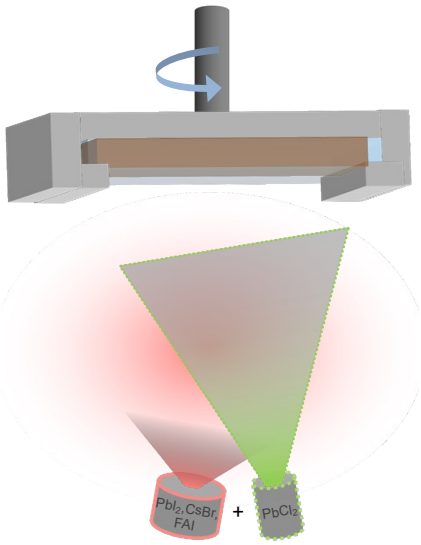

Fig. S1 Sketch of depositing perovskite by thermal evaporation showing the idea of introducing $PbCl_2$ additive to the vapor formed by sublimating PbI_2, CsBr and FAI. Note: in this sketch we depict PbI_2, CsBr and FAI sources as one integrated single source for clearly showing the idea of introducing $PbCl_2$ to the vapor. Actually, they are 3 separate and independently controlled sources.

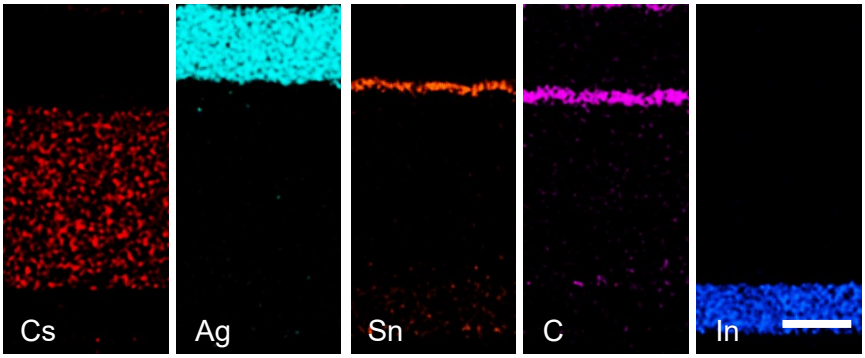

Fig. S2 STEM-EDX mappings for Cs, Ag, Sn, C, and In elements. Note: The images are sharing the same scale bar shown on In mapping, with a length of 100 nm.

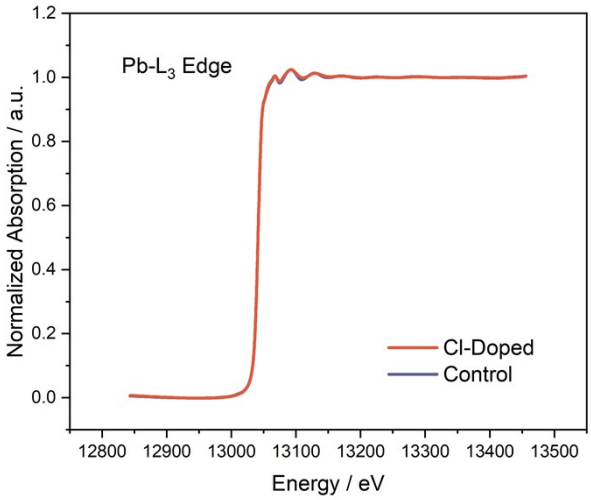

Fig. S3 EXAFS spectra of Pb-L_3 edge of perovskites without and with Cl-doping measured in transmission mode.

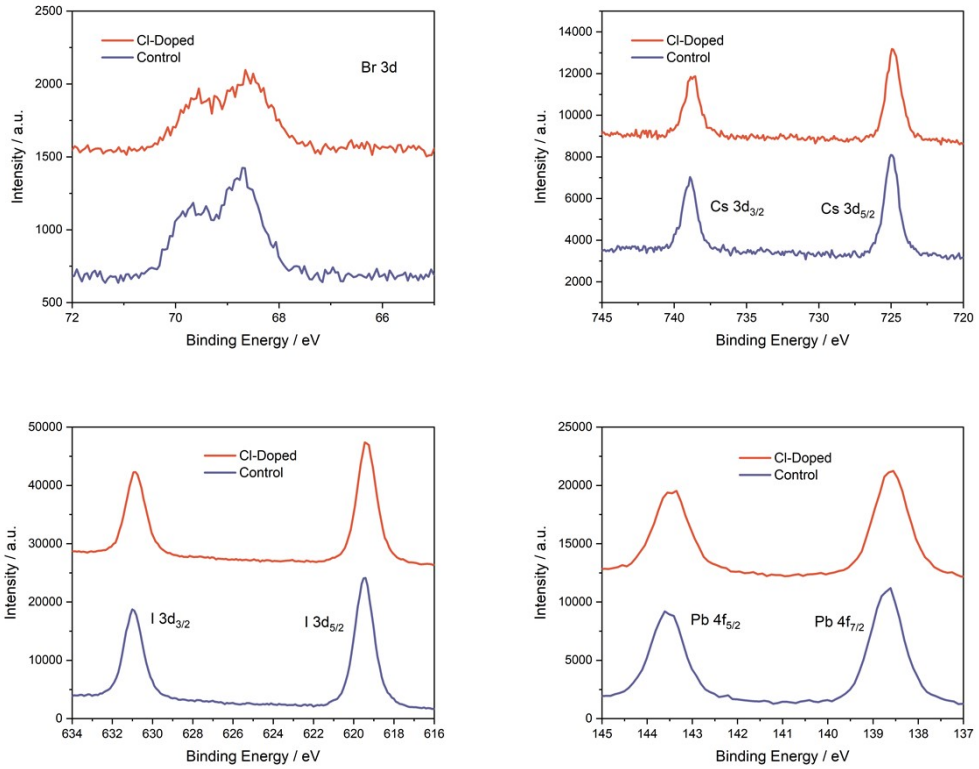

Fig. S4 Br 3d, Cs 3d, I 3d, and Pb 4f XPS results of perovskites without and with Cl-doping. Note: All XPS results are calibrated by fixing the C 1s peak at 284.8 eV.

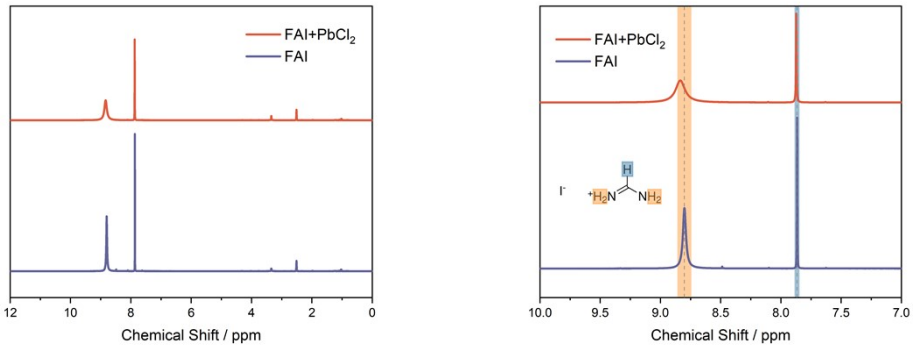

Fig. S5 ^{1}H-NMR results of FAI without and with $PbCl_2$ mixed in full range (left) and zoomed-in range of 10.0 to 7.0 ppm (right). Note: FAI: ^{1}H NMR (400 MHz, DMSO-d_6) δ 8.80 (s, 4H), 7.87 (s, 1H). FAI+$PbCl_2$: ^{1}H NMR (400 MHz, DMSO-d_6) δ 8.84 (s, 4H), 7.87 (s, 1H). These results are calibrated by fixing the solvent residual signals of DMSO-d_6 at 2.50 ppm.[S4]

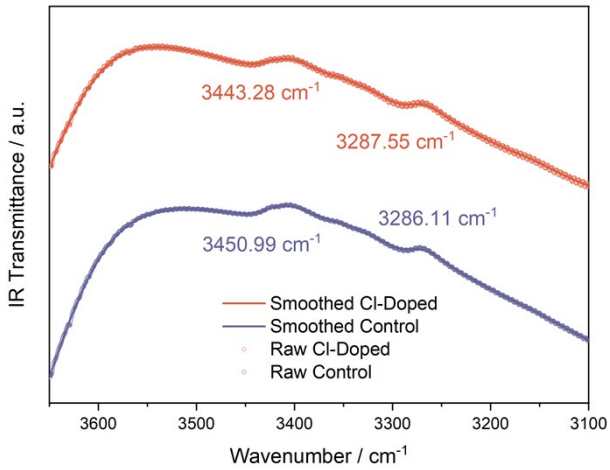

Fig. S6 FTIR results of perovskite without and with Cl-doping. Note: The two peaks identified and marked are within N-H stretching (~3450 cm^{-1}) and C-H stretching (~3290 cm^{-1}) zones, respectively.

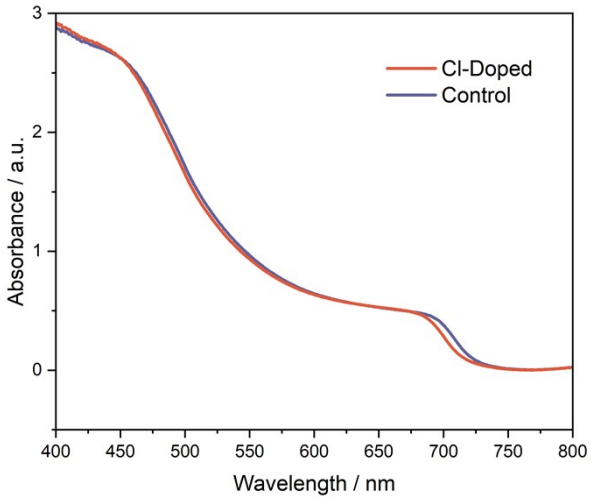

Fig. S7 UV-vis absorption spectra of perovskites without and with Cl-doping.

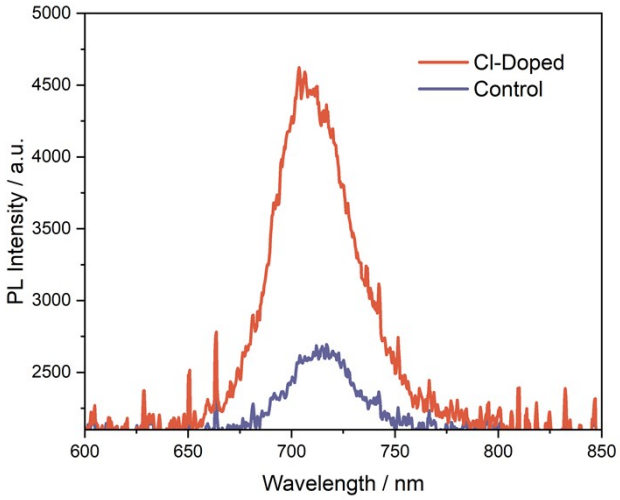

Fig. S8 Raw steady-state PL spectra of perovskite thin-films without and with Cl-doping, without smoothing.

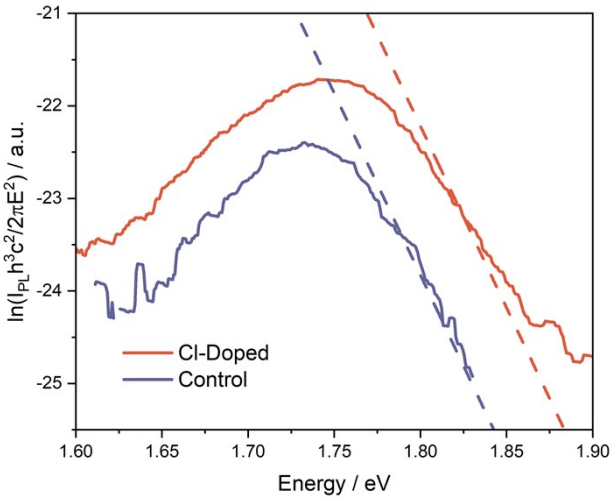

Fig. S9 Fitting QFLS values for perovskite thin-films without and with Cl-doping.

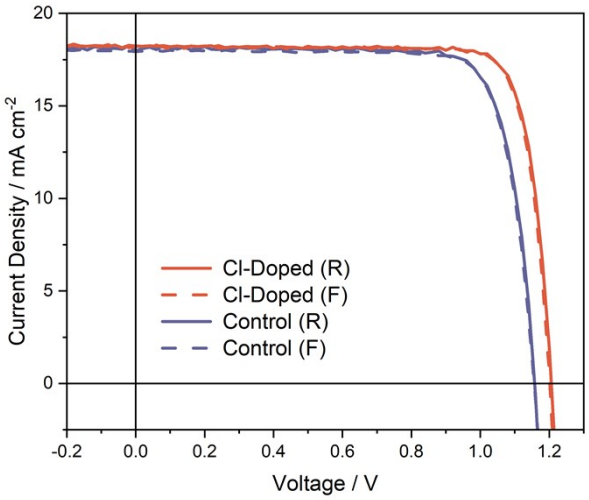

Fig. S10 Champion *J-V* curves in forward and reverse scan directions for single-junction wide-bandgap PSCs without and with Cl-doping. Note: "F" denotes forward scan and "R" denotes reverse scan.

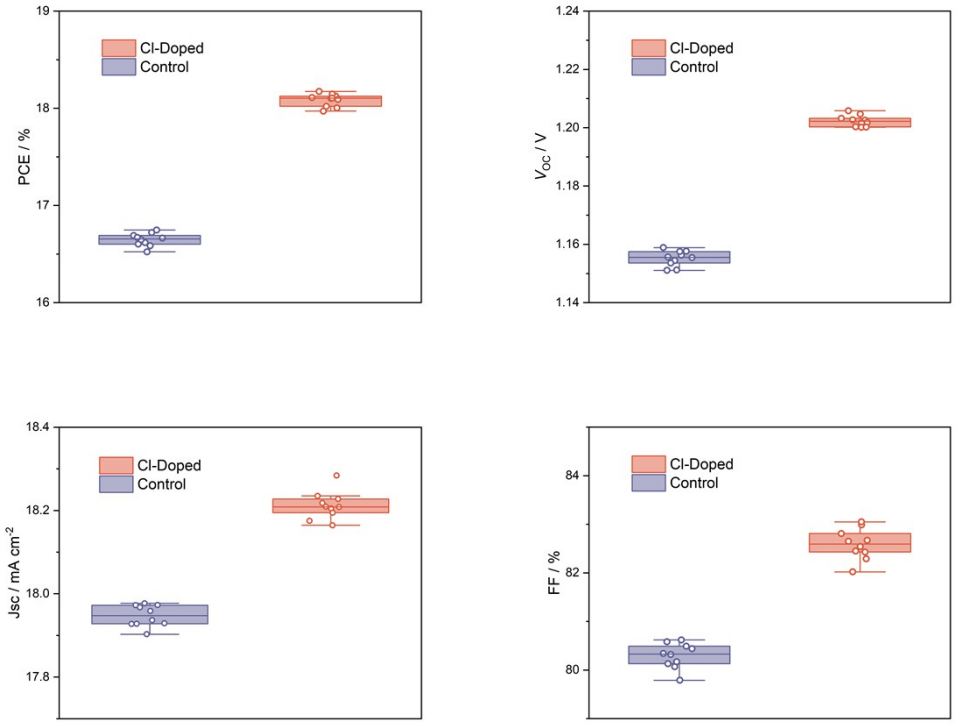

Fig. S11 Statistics of PCE, V_{OC}, J_{SC}, and FF from 10 single-junction wide-bandgap PSCs without and with Cl-doping. Note: From highest to lowest of bars and boxes: maximum, 75th percentile, median, 25th percentile, and minimum.

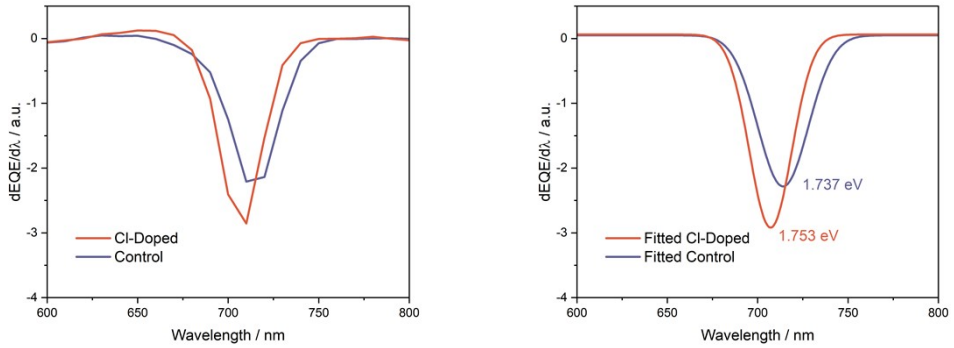

Fig. S12 Photovoltaic bandgaps determined by inflection points of EQE curves for single-junction wide-bandgap PSCs without and with Cl-doping. Note: the left figure shows raw dEQE/dλ curve while the right figure shows the fitted curve by Gaussian function, for the ease of determination of photovoltaic bandgaps.

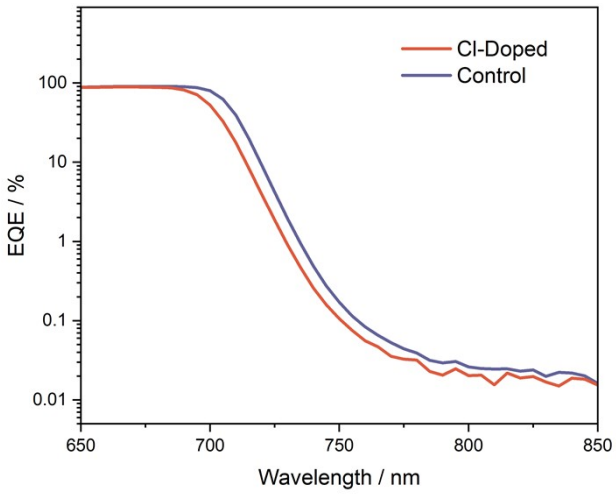

Fig. S13 HREQE curves of single-junction wide-bandgap PSCs without and with Cl-doping.

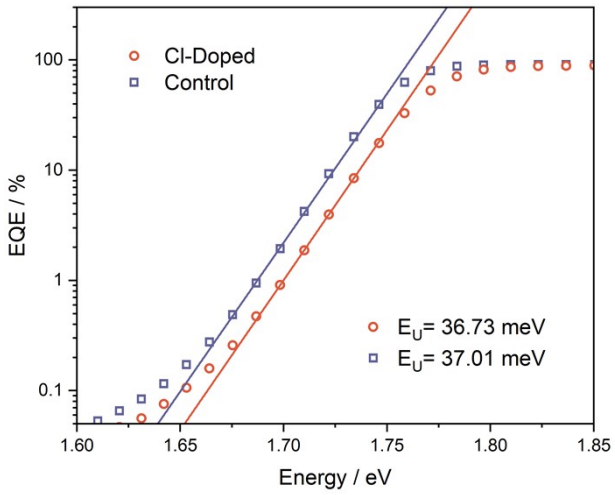

Fig. S14 Fitting Urbach energies for single-junction wide-bandgap PSCs without and with Cl-doping.

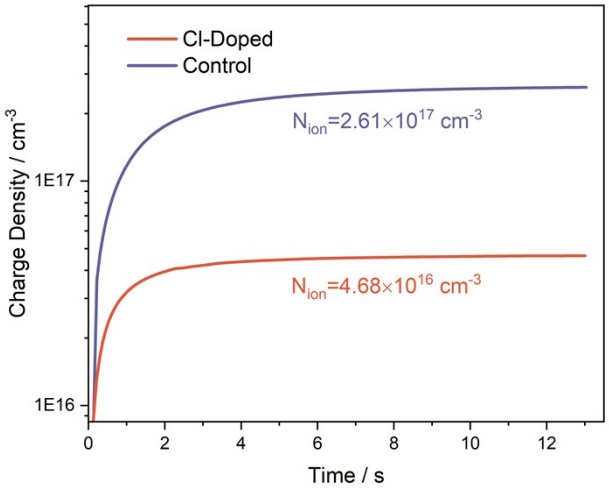

Fig. S15 Calculating mobile ion concentrations through BACE method for single-junction wide-bandgap PSCs without and with Cl-doping.

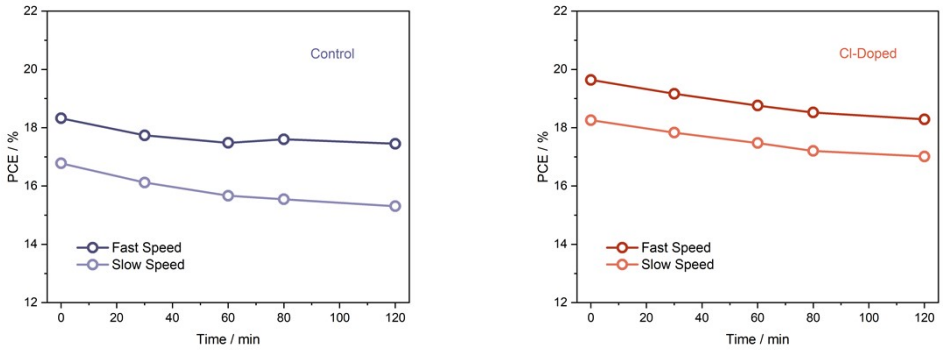

Fig. S16 Evolution of PCEs obtained from slow and fast *J-V* scan speeds for single-junction wide-bandgap PSCs without (left) and with (right) Cl-doping during 120 minutes' aging.

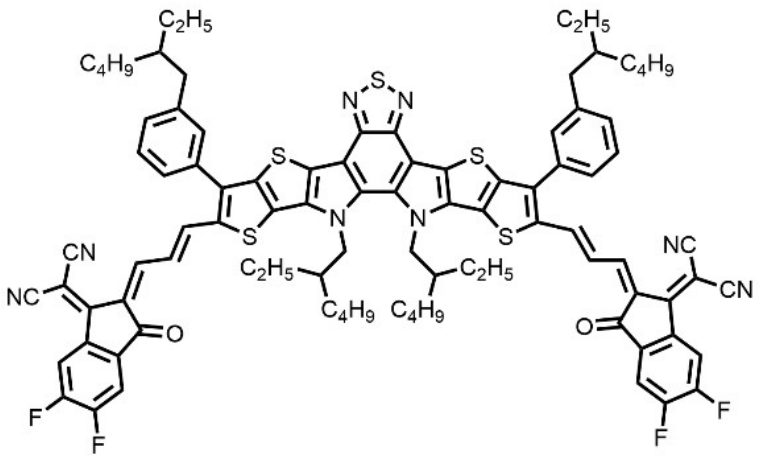

Fig. S17 Molecular structure of P2EH-2V narrow-bandgap non-fullerene acceptor.

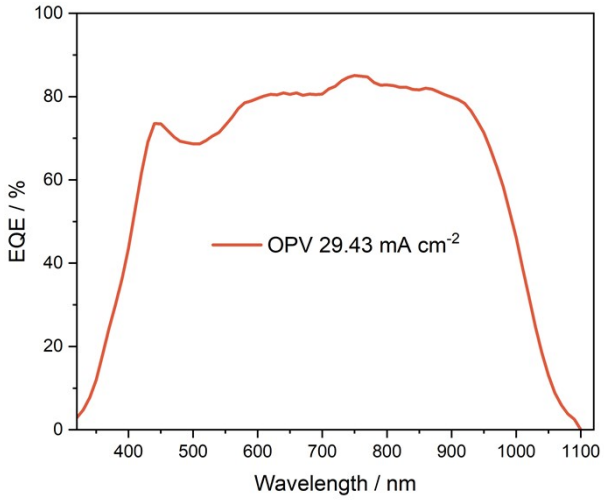

Fig. S18 EQE curve and integrated J_{SC} value of single-junction OPV solar cell.

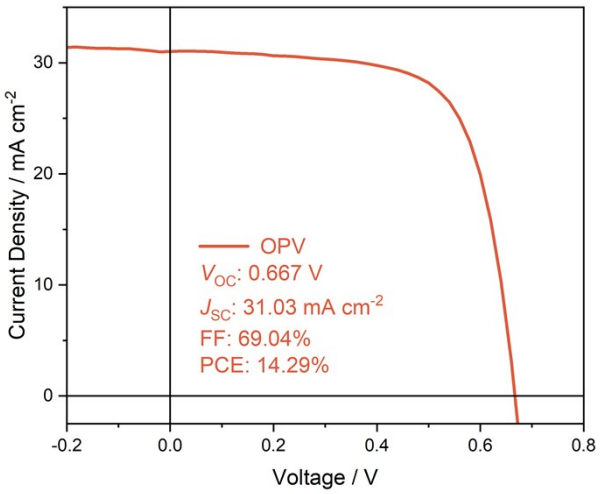

Fig. S19 Champion *J-V* curve and photovoltaic parameters for single-junction OPV solar cell.

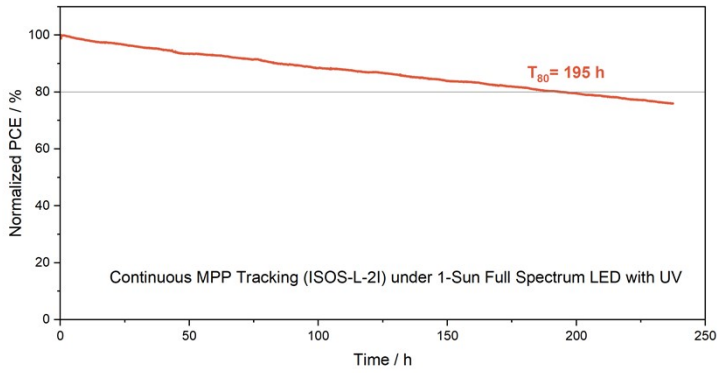

Fig. S20 MPP stability tracking result for perovskite-OPV TSC at 65°C with temperature controlling under 1-sun full spectrum (350-900 nm with UV) white LED light illumination in a N_2-filled glovebox.

Table S1. Summary of atomic ratios of Pb, I, and Cl elements determined from STEM-EDX mappings.

	Pb	I	Cl
Atomic Ratio / %	22.61	52.06	0.54

Table S2. Summary of reported MPP stability results (remained PCE vs. time elapsed) of perovskite-based thin-film TSCs. Note: "P-O" denotes perovskite-OPV, "P-P" denotes perovskite-perovskite and "P-C" denotes perovskite-CIGS TSCs.

Tandem Type	Temperature	PCE Remained / %	Time / h	Reference
P-O	No Control	90	500	*Nat. Energy* **7**, 229-237 (2022)
P-O	N/A	80	130	*Nature* **604**, 280-286 (2022)
P-O	~55°C	81	1000	*Small* **18**, 2204081 (2022)
P-O	45~55°C	86	1000	*Adv. Mater.* **35**, 2208604 (2023)
P-O	N/A	90	500	*Adv. Mater.* **35**, 2305946 (2023)
P-O	N/A	90	200	*Energy Environ. Sci.* **17**, 1046-1060 (2024)
P-O	~45°C	90	500	*Nat. Energy* **9**, 411-421 (2024)
P-O	45°C	90	1000	*Angew. Chem. Int. Ed.* **63**, e202412515 (2024)
P-O	N/A	80	540	*Adv. Energy Mater.* **14**, 2400691 (2024)
P-O	N/A	93	700	*Nature* **635**, 860-866 (2024)
P-O	N/A	80	200	*Energy Environ. Sci.* **17**, 9580-9589 (2024)
P-O	25°C	80	381	*Joule* **8**, 2554-2569 (2024)
P-O	45~55°C	87	1000	*Adv. Mater.* **37**, 2411027 (2025)
P-O	N/A	90	450	*Nat. Commun.* **16**, 1773 (2025)
P-O	35~45°C	84	650	*Nat. Commun.* **16**, 2759 (2025)
P-O	N/A	80	350	*Adv. Mater.*, 2500190 (2025)
P-O	40°C	80	305	*Adv. Energy*

				Mater., 2404092 (2025)
P-O	40~50°C	85	1000	*Nat. Energy* **10**, 513-525 (2025)
P-O	45°C	80	500	*Energy Environ. Sci.* **18**, 4883-4892 (2025)
P-P	54~60°C	88	500	*Nat. Energy* **5**, 870-880 (2020)
P-P	65°C	80	900	*Sol. RRL* **5**, 2100814 (2021)
P-P	N/A	75	500	*Science* **376**, 762-767 (2022)
P-P	35°C	90	600	*Nature* **603**, 73-78 (2022)
P-P	N/A	90	450	*Nat. Energy* **7**, 744-753 (2022)
P-P	30~35°C	80	1500 (0.8 sun)	*Nat. Energy* **7**, 642-651 (2022)
P-P	25°C	90	500	*Angew. Chem. Int. Ed.* **62**, e202313374 (2023)
P-P	35°C	93	600	*Nature* **620**, 994-1000 (2023)
P-P	55°C	80	380	*Nature* **624**, 69-73 (2023)
P-P	N/A	80	415	*Nature* **618**, 80-86 (2023)
P-P	N/A	86	500	*Nature* **613**, 676-681 (2023)
P-P	~50°C	80	656	*Science* **383**, 855-859 (2024)
P-P	25°C	80	352	*Adv. Mater.* **36**, 2308706 (2024)
P-P	25°C	80	370	*Nat. Energy* **9**, 298-307 (2024)
P-P	40~45°C	90	750	*Nat. Mater.* **24**, 252-259 (2025)
P-P	N/A	80.5	300	*Adv. Mater.* **37**, 2415627 (2025)
P-P	N/A	75	600	*Nat. Energy* **10**, 318-328 (2025)
P-P	55°C	90	663	*Nat. Nanotechnol.*

				20, 764-771 (2025)
P-P	N/A	90	500	*Nat. Commun.* **16**, 4148 (2025)
P-P	N/A	87.3	800	*Energy Environ. Sci.* **18**, 5503-5510 (2025)
P-C	30°C	88	500	*Science* **361**, 904-908 (2018)
P-C	35°C	85	280	*Joule* **9**, 101794 (2025)
P-C	N/A	77	400	*Adv. Energy Mater.* **15**, 2403682 (2025)
P-O	**~45°C**	**80**	**1979**	**This Work**

Note S1. Calculation of $PbCl_2$ amount incorporated with PbI_2 as a 100% reference according to Cl:Pb ratio determined from STEM-EDX.

From the STEM-EDX data in Table S1, the Cl:Pb ratio is determined as 2.39%. In the deposited perovskite film, Cl element is from incorporated $PbCl_2$ while Pb element is from both of $PbCl_2$ and PbI_2. If PbI_2 is set as a 100% reference and the $PbCl_2$ amount in molar ratio is assumed to be x, then we have:

$$\frac{2x}{1+x} = 2.39\%$$

The x is then solved as 1.21%, corresponding to the incorporated $PbCl_2$ amount in molar ratio with PbI_2 as a 100% reference.

References

S1. N. Kalasariya, P. F. Sowmeeh, F. Pena-Camargo, F. Vanin, T. Lukas, Y. Dong, Q. Feng, Z. Liu, W. A. Memon, D. Gao, J. Gong, X. Wu, A. F. C. Mendez, J. Hagenberg, Z. Abadi, T. Hultzsch, X. Zhao, S. Shah, H. Yu, V. Srivastava, J. Xu, N. Zhao, F. Lang, Z. Zhu and M. Stolterfoht, *Adv. Energy Mater.*, 2026, e03866.

S2. S. Kraft, J. Stümpel, P. Becker and U. Kuetgens, *Rev. Sci. Instrum.*, 1996, **67**, 681–687.

S3. B. Ravel and M. Newville, *J. Synchrotron Rad.*, 2005, **12**, 537-541.

S4. G. R. Fulmer, A. J. M. Miller, N. H. Sherden, H. E. Gottlieb, A. Nudelman, B. M. Stoltz, J. E. Bercaw and K. I. Goldberg, *Organometallics*, 2010, **29**, 2176–2179.